



Effective extraction of photoneutron cross-section distribution using gamma activation and reaction yield ratio method

Zhi-Cai Li¹ · Yue Yang² · Zong-Wei Cao¹ · Xin-Xiang Li¹ · Yun Yuan¹ · Zong-Qing Zhao² · Gong-Tao Fan³ · Hong-Wei Wang³ · Wen Luo¹

Received: 18 June 2023 / Revised: 25 August 2023 / Accepted: 25 August 2023 / Published online: 18 November 2023

© The Author(s), under exclusive licence to China Science Publishing & Media Ltd. (Science Press), Shanghai Institute of Applied Physics, the Chinese Academy of Sciences, Chinese Nuclear Society 2023

Abstract

Photoneutron cross-section (PNCS) data are important in various current and emerging applications. Although a few sophisticated methods have been developed, there is still an urgent need to study the PNCS data. In this study, we propose the extraction of PNCS distributions using a combination of gamma activation and reaction yield ratio methods. To verify the validity of the proposed extraction method, experiments for generating $^{62,64}\text{Cu}$ and $^{85\text{m},87\text{m}}\text{Sr}$ isotopes via laser-induced photoneutron reactions were performed, and the reaction yields of these isotopes were obtained. Using the proposed extraction method, the PNCS distributions of ^{63}Cu and ^{86}Sr isotopes (leading to $^{85\text{m}}\text{Sr}$ isotope production) were successfully extracted. These extracted PNCS distributions were benchmarked against available PNCS data or TALYS calculations, demonstrating the validity of the proposed extraction method. Potential applications for predicting the PNCS distributions of the 30 isotopes are further introduced. We conclude that the proposed extraction method is an effective complement to the available sophisticated methods for measuring and evaluating PNCS data.

Keywords Photoneuclear data · Photoneutron cross section · Gamma activation · Reaction yield · TALYS calculation

1 Introduction

Photonuclear data describe the interactions between photons and atomic nuclei. They are primarily composed of photoneutron cross-section (PNCS) data and photocharged-particle cross-section data. They play a vital role in a wide

range of current and emerging applications [1]. These applications include radiation shielding design, radiation transport analysis [2], absorbed dose calculations in the human body during radiotherapy, fission and fusion reactor physics and technology [3, 4], activation analyses, safeguards and inspection technologies, medical isotope production [5, 6], nuclear waste transmutation, and astrophysical nucleosynthesis [7, 8]. In the field of medical isotope production, the PNCS data can guide the production of radioisotopes for diagnostic and therapeutic purposes [9, 10]. With the advent of new facilities that produce brilliant and intense photon beams, the photoproduction of neutron-deficient isotopes could become a competitive alternative to traditional methods that use neutrons generated by nuclear reactors or charged particle beams [11–13].

PNCS data have been experimentally obtained from various types of measurements, with bremsstrahlung and quasi-monoenergetic photons from positron annihilation in flight, and more recently, from laser Compton scattering (LCS) [14–16]. Most existing experimental data correlate with studies on PNCSs. Although PNCSs are obtained by counting the total number of emitted neutrons, the determination of partial

This work was supported by the National Key R & D Program of China (No. 2022YFA1603300), the National Natural Science Foundation of China (Nos. U2230133), the Independent Research Project of the Key Laboratory of Plasma Physics, CAEP (No. JCKYS2021212009), the Open Fund of the Key Laboratory of Nuclear Data, CIAE (No. JCKY2022201C152), and Hengyang Municipal Science and Technology Project (No.202150054076).

✉ Wen Luo
wenluo-ok@163.com

¹ School of Nuclear Science and Technology, University of South China, Hengyang 421001, China

² Science and Technology on Plasma Physics Laboratory, Laser Fusion Research Center, China Academy of Engineering Physics, Mianyang 621900, China

³ Shanghai Advanced Research Institute, Chinese Academy of Sciences, Shanghai 201210, China

PNCSs requires neutron multiplicity sorting [17]. One advantage of bremsstrahlung measurements [18] is the high photon beam intensity. However, the technique has several disadvantages. First, it is necessary to know the bremsstrahlung spectrum sufficient for all electron energies. Next, measuring the reaction yield curve in a small energy step requires a stable accelerator and large counting statistics. Third, the process of subtracting the yield curves in the unfolding procedure may introduce correlations between the experimental data points, which can lead to fluctuations in the unfolded cross sections. In contrast to bremsstrahlung measurements employing a mathematical approach, positron annihilation in flight and LCS offered an apparatus method for producing them with variable energies [19, 20]. However, the effective spectrum of the incident photon beam should be known in advance. Consequently, all these measurements require a precise scan of the incident photon energy and accurate knowledge of the incident photon spectrum and beam intensity.

Regarding the evaluation of the PNCS, the International Atomic Energy Agency has organized two coordinated research projects and photonuclear data of 219 isotopes were evaluated successfully because of the growing need for photonuclear data [21, 22]. Despite the available experimental and evaluation efforts on photonuclear data, there is still an urgent need to study PNCS data for the following three reasons: (a) there is a lack of data for a number of cases; (b) it is not possible to produce a complete PNCS data file based on measured PNCSs alone; and (c) the experimental PNCS data often suffer from systematic discrepancies that are not easy to resolve [1].

In this study, we propose an effective method for the extraction of PNCS distributions using gamma activation and the reaction yield ratio method. Note that gamma activation can be accomplished through either laser plasma-based bremsstrahlung radiation or LCS photon irradiation of a solid target. This extraction method was verified by reasonably reproducing the experimental/evaluated and calculated PNCS data and can potentially be used to predict the PNCS distributions of 30 stable isotopes. The remainder of this study is organized as follows: in Sect. 2, the extraction method is introduced to obtain the peak cross sections and further predict PNCS distributions. The benchmark results obtained using the extraction method are presented in Sect. 3. The merits of the extraction method and the possibility of predicting PNCS distributions for 30 isotopes are discussed in Sect. 4. The conclusions and outlook are presented in Sect. 5.

2 Extraction of PNCS distribution

Relativistic laser-plasma interactions are bright, incoherent sources of gamma radiation with energies up to several tens of megaelectronvolts. They can be produced by compact

tabletop laser systems that deliver laser pulses with energies of less than 100 fs. The spectra of the laser-accelerated electrons and bremsstrahlung photons can be described by the Boltzmann distribution [23]

$$n_{e,\gamma}(E) = \frac{n_{e,\gamma}(0)}{k_B T_{e,\gamma}} \exp \left\{ -E/k_B T_{e,\gamma} \right\}, \quad (1)$$

where $T_{e,\gamma}$ is the electron or photon temperature, k_B is the Boltzmann's constant, and $n_{e,\gamma}(0)$ is the number of electrons or photons within the energy bin at $E_{e,\gamma} = 0$ MeV. It can be seen that the intensity of laser-accelerated electrons or bremsstrahlung photons decreases exponentially with energy. The threshold energies E_{th} are generally a few MeV for photoneutron reactions. To efficiently trigger such reactions, the photon temperature T_γ must reach the MeV/ k_B .

For nuclides with a single giant dipole resonance (GDR) peak, the PNCS distribution can be described by a Lorentzian-like shape [24].

$$\sigma(E) = \frac{\sigma_m}{1 + [(E^2 - E_m^2)^2 / E^2 \Gamma^2]}, \quad (2)$$

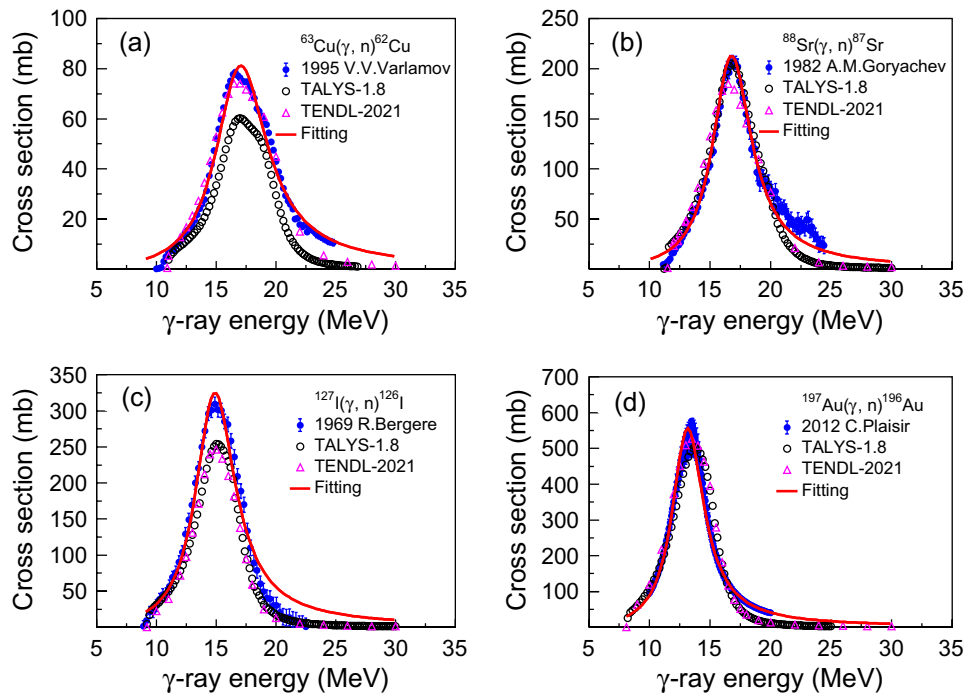
where the peak energy E_m , peak cross section σ_m and width Γ are the three Lorentzian distribution parameters. These parameters can be acquired from TALYS calculations, TENDL evaluations, and experimental data available in the EXFOR database. Figure 1 shows that the Lorentzian curves accurately reproduce the experimental PNCSs for the four representative nuclides: ^{63}Cu , ^{88}Sr , ^{127}I , and ^{197}Au . The TALYS calculation underestimated the measured σ_m values for ^{63}Cu and ^{127}I , whereas the TENDL evaluations aligned with the experimental data. In addition, visible discrepancies were found between the experimental data and the TENDL evaluations.

The reaction yield Y depends on the temperature T_γ and cross section $\sigma(E)$. The expression for the reaction yield Y can be written as:

$$Y = \frac{nd}{k_B T_\gamma} \int \sigma(E) n_\gamma(0) \exp \left\{ -E/k_B T_\gamma \right\} dE, \quad (3)$$

where n is the number of target nuclei per unit area, and d is the thickness of the target. For a specific target comprising isotopes A and B irradiated by a laser-generated bremsstrahlung photon beam, the residual nuclei A' and B' are produced through photoneutron reactions. When isotopes A and B have very similar mass numbers, their PNCS distributions could be very close in terms of peak energy E_m and width Γ but vary in terms of the peak cross section σ_m . Figure 2 shows the PNCS distributions of Cu, Sr, I, and Au nuclei, whose isotopes have three adjacent mass numbers. The three Lorentzian parameters of their PNCS distributions are listed in Table 1. It can be seen that, although the peak cross sections

Fig. 1 (Color online) PNCS distributions of four nuclides ^{63}Cu , ^{88}Sr , ^{127}I and ^{197}Au . Experimental data in the figure are taken from Refs. [24–27]. The hollow black circle and hollow pink triangle indicate the (γ, n) cross sections obtained with TALYS (version 1.8) calculations and TENDL (2021) evaluations [28], respectively. The red line shows the Lorentzian curve fitted with Eq. (2)



σ_m for these nuclides with adjacent mass numbers have large relative differences of 10–30%, the peak energies E_m are very close to each other because their relative differences are lower than 3%, and the relative deviation of the width Γ is approximately 10%. Substituting Eq. (2) into Eq. (3), the isotope yield ratio can be written as

$$\begin{aligned} \frac{Y_{A'}}{Y_{B'}} &= \frac{n_A}{n_B} \cdot \frac{\int \sigma_A(E) \exp\{-E/k_B T_\gamma\} dE}{\int \sigma_B(E) \exp\{-E/k_B T_\gamma\} dE} \\ &= \frac{n_A}{n_B} \cdot \frac{\sigma_{mA}}{\sigma_{mB}} \cdot \frac{\int \frac{\exp\{-E/k_B T_\gamma\}}{1+[(E^2-E_{mA}^2)^2/E^2\Gamma_A^2]} dE}{\int \frac{\exp\{-E/k_B T_\gamma\}}{1+[(E^2-E_{mB}^2)^2/E^2\Gamma_B^2]} dE} \\ &\approx \frac{n_A}{n_B} \cdot \frac{\sigma_{mA}}{\sigma_{mB}}. \end{aligned} \tag{4}$$

Fig. 2 (Color online) PNCS distributions of $^{62-64}\text{Cu}$ isotopes (a), $^{87-89}\text{Sr}$ isotopes (b), $^{126-128}\text{I}$ isotopes (c), and $^{196-198}\text{Au}$ isotopes (d) computed with TALYS software (version 1.8). Note that experimental data for these PNCS distributions are not available, and the TALYS calculations are used for showing the difference of the PNCS distributions of adjacent isotopes

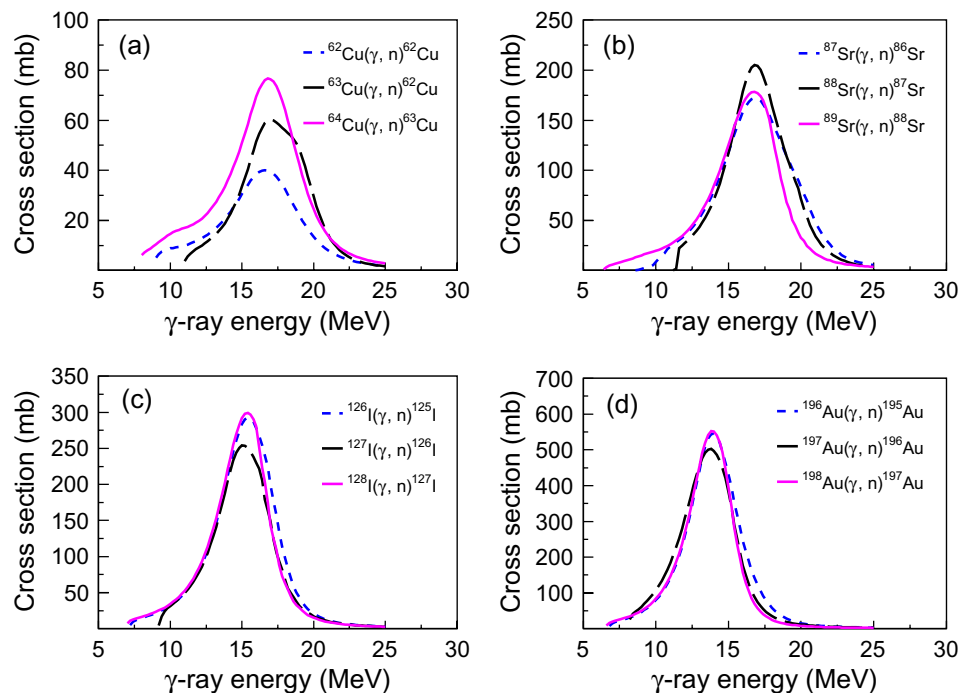


Table 1 Lorentzian parameters for photoneutron reactions on Cu, Sr, I and Au nuclei

Reaction	Lorentzian parameters		
	E_m (MeV)	Γ (MeV)	σ_m (mb)
$^{62}\text{Cu}(\gamma, n)^{61}\text{Cu}$	16.25 ± 0.05	5.05 ± 0.12	41.16 ± 0.67
$^{63}\text{Cu}(\gamma, n)^{62}\text{Cu}$	17.13 ± 0.05	4.42 ± 0.13	64.60 ± 1.37
$^{64}\text{Cu}(\gamma, n)^{63}\text{Cu}$	16.52 ± 0.04	4.65 ± 0.11	78.30 ± 1.39
$^{87}\text{Sr}(\gamma, n)^{86}\text{Sr}$	16.72 ± 0.04	4.79 ± 0.09	180.70 ± 2.43
$^{88}\text{Sr}(\gamma, n)^{87}\text{Sr}$	16.78 ± 0.04	3.95 ± 0.10	212.89 ± 3.63
$^{89}\text{Sr}(\gamma, n)^{88}\text{Sr}$	16.34 ± 0.04	3.98 ± 0.09	187.40 ± 3.07
$^{126}\text{I}(\gamma, n)^{125}\text{I}$	15.23 ± 0.03	3.67 ± 0.08	309.81 ± 4.57
$^{127}\text{I}(\gamma, n)^{126}\text{I}$	14.96 ± 0.05	3.68 ± 0.11	268.98 ± 5.88
$^{128}\text{I}(\gamma, n)^{127}\text{I}$	15.02 ± 0.03	3.37 ± 0.08	313.65 ± 4.87
$^{196}\text{Au}(\gamma, n)^{195}\text{Au}$	13.83 ± 0.02	3.08 ± 0.06	571.62 ± 6.50
$^{197}\text{Au}(\gamma, n)^{196}\text{Au}$	13.51 ± 0.03	3.40 ± 0.08	534.44 ± 8.31
$^{198}\text{Au}(\gamma, n)^{197}\text{Au}$	13.68 ± 0.03	2.92 ± 0.06	584.38 ± 8.81

Because of the complexity of the integral ratio in Eq. (4), we cannot deduce the integral ratio directly; thus, an approximate expression is provided. To verify the validity of the approximation, the integral ratio was calculated using the summation method (i.e., the integral was replaced by the summation). Considering the slope temperature of the photon spectrum $T_\gamma = 5 \text{ MeV}/k_B$ (which can be readily achieved by state-of-the-art laser plasma-based bremsstrahlung sources [29, 30]), the integral ratio is approximated to be 1.0 and the root mean square deviation is 0.067, which is calculated over a wide range of A and Z (note that $26 < Z < 81$ and for a certain nuclide, four nuclides with mass numbers adjacent to A are considered). This deviation correlates with the relative differences between E_m and Γ . Consequently, we consider 6.7% as the systematic uncertainty of the proposed extraction method.

After irradiating a target composed of isotopes A and B with laser-generated bremsstrahlung photons, γ -ray counting was performed for residual nuclei A' and B' . The γ lines unique to the residual nuclei are clearly identified in the γ -ray spectra, which are generally measured using an energy- and efficiency-calibrated high-purity germanium (HPGe) detector. The reaction yields $Y_{A'}$ and $Y_{B'}$ were obtained using the γ -ray spectrum. For example, the expressions for $Y_{A'}$ or $Y_{B'}$ are as follows [31]:

$$Y_{A', B'} = \frac{N_{\text{det}}(t_r/t_m)}{I_\gamma \epsilon k_e (1 - e^{-\lambda t_m}) e^{-\lambda t_c}} \quad (5)$$

where N_{det} is the peak count of characteristic γ rays used to identify the residual nuclei, t_r is the time for real measurement, t_m is the measurement time, t_c is the cooling time, I_γ is the branching intensity, ϵ is the source-peak detection

efficiency, and $k_e = \frac{1 - e^{-\mu d}}{\mu d}$ is the correction factor for the self-absorption of the characteristic γ rays in the sample thickness d with absorption coefficient μ . According to Eq. (4), the peak cross sections $\sigma_{m,A}$ can be obtained as follows:

$$\sigma_{m,A} = \frac{Y_{A'}}{Y_{B'}} \cdot \frac{n_B}{n_A} \cdot \sigma_{m,B}. \quad (6)$$

This indicates that when the distribution of the PNCS is known for isotope B (or A), the distribution of the PNCS for isotope A (or B) can be readily extracted if their peak energies E_m and widths Γ are very close to each other. The above method used to extract the PNCS distribution is valid only for nuclei with a single GDR peak. In the case of deformed nuclei, the GDR peak may split into two, where each corresponds to the major or minor axis of the ellipsoid [19], and the resulting $\sigma(E)$ is given by the sum of the two GDR peaks, which complicates the proposed extraction method.

3 Benchmarking results

To verify the aforementioned extraction method using gamma activation and the isotope yield ratio, experiments for generating $^{62,64}\text{Cu}$ and $^{85\text{m}, 87\text{m}}\text{Sr}$ isotopes via laser-induced photoneuclear reactions were performed at the Xing-Guang III laser facility of the Laser Fusion Research Center (LFRC) at Mianyang. Large-charge megaelectronvolt electron (e^-) beams were generated using 100 TW picosecond (ps) laser pulses. The e^- beams then impinge on metal stacks composed of a Ta foil and activation plates (Cu or SrCl target) of interest, producing high-energy bremsstrahlung radiation and isotopes $^{62,64}\text{Cu}$ or $^{85\text{m}, 87\text{m}}\text{Sr}$. The bremsstrahlung radiations produced have a Boltzmann-like distribution with $T_\gamma \approx 4.6 \text{ MeV}/k_B$. The obtained reaction yields of $Y_{62,64\text{Cu}}$ are obtained 4.86×10^6 and 2.65×10^6 per laser shot, respectively [32]. The reaction yields $Y_{85\text{m}, 87\text{m}\text{Sr}}$ were determined to be 1.8×10^4 and 2.1×10^5 per laser shot, respectively. In the following section, we introduce how to obtain the peak cross sections of the isotopes of interest and then predict the PNCS distributions for two exemplary isotopes, ^{63}Cu and ^{86}Sr .

3.1 PNCS distribution of ^{63}Cu

The half-lives of $^{62,64}\text{Cu}$ isotopes are 9.7 min and 12.7 h, respectively. They have principle characteristic emissions $E_\gamma = 511.0 \text{ keV}$ with branching intensity $I_\gamma = 195.7\%$ for ^{62}Cu and of $I_\gamma = 35.2\%$ for ^{64}Cu . Although the $^{62,64}\text{Cu}$ isotopes have the same characteristic emissions at 511 keV, their reaction yields can be reasonably extracted because of the significant differences in their half-lives [32]. According to the experimental reaction yields $Y_{62,64\text{Cu}}$ and the natural

abundance of Cu isotopes, the ratio of the peak cross section $\sigma_{m,63Cu}/\sigma_{m,65Cu}$ was obtained as 0.82. Experimental cross-sectional data [17] and evaluated data (IAEA-2019) [33] are available for $^{65}Cu(\gamma, n)$ reaction, as shown in Fig. 3a. The Lorentzian-like shape of Eq. (2) was used to fit the data. The Lorentzian parameters ($E_{m,65,63Cu}$, $\sigma_{m,65,63Cu}$, and $\Gamma_{65,63Cu}$) were then obtained (see Table 2). Using experimental and evaluated PNCS data, the $\sigma_{m,65Cu}$ are fitted to be 96.63 mb and 93.03 mb, respectively. According to Eq. (6), the peak cross sections $\sigma_{m,63Cu}$ were obtained as 79.24 ± 5.44 mb and 76.28 ± 5.24 mb, respectively. Finally, the PNCS distribution for ^{63}Cu can be predicted by the three Lorentzian parameters $E_{m,65Cu}$, $\sigma_{m,63Cu}$, and Γ_{65Cu} (or Γ_{63Cu} when available). Figure 3b shows two PNCS distributions for ^{63}Cu (i.e., PNCS #1 and PNCS #2), which were extracted from the Lorentzian parameters fitted from the experimental and evaluated data of ^{65}Cu , respectively. The experimental and evaluated PNCS data for ^{63}Cu are shown in Fig. 3b. The uncertainty of the predicted PNCS distribution for ^{63}Cu was obtained using the error propagation formula, considering a statistical uncertainty of 1.5% of the measured $Y_{62,64Cu}$ and a systematic uncertainty of 6.7% induced by the proposed extraction method. PNCS #1 and PNCS #2 have an uncertainty of 6.9%. The benchmark results show that the extracted PNCS distribution is consistent with the evaluated data (IAEA-2019). Consequently, the validity of the proposed extraction method was confirmed.

3.2 PNCS distribution of ^{86}Sr (leading to ^{85m}Sr isotope production)

The half-lives of $^{85m}, ^{87m}Sr$ isotopes are 67.6 min and 2.8 h, respectively. They have principle characteristic emissions $E_{\gamma} = 231.9$ keV with branching intensity $I_{\gamma} = 83.9\%$ for ^{85m}Sr and $E_{\gamma} = 388.5$ keV with $I_{\gamma} = 82.2\%$ for ^{87m}Sr . Similarly, the ratio of the peak cross section $\sigma_{m,86Sr}/\sigma_{m,88Sr}$ was 0.72. Because experimental PNCS data were not available for $^{88}Sr(\gamma, n)^{87m}Sr$ and $^{86}Sr(\gamma, n)^{85m}Sr$ reactions, TALYS calculations were performed, and the calculated curves are shown in Fig. 4a. These curves were then fitted to a Lorentzian-like shape, and the obtained Lorentzian parameters ($E_{m,86,88Sr}$, $\sigma_{m,86,88Sr}$, and $\Gamma_{86,88Sr}$) are listed in Table 3. The fitted $\sigma_{m,88Sr}$ is 163.13 mb. According to Eq. (6), the peak cross section $\sigma_{m,86Sr}$ was obtained to be 117.11 ± 7.96 mb, respectively. Finally, the PNCS distribution of ^{86}Sr can be predicted using the following three Lorentzian parameters: $E_{m,88Sr}$, $\sigma_{m,86Sr}$ and Γ_{88Sr} . The results are presented in Fig. 4b. The cross-sectional data for the $^{86}Sr(\gamma, n)^{85m}Sr$ reaction were calculated using the TALYS software and are also shown in Fig. 4b. Similarly, the uncertainty in the predicted PNCS distribution for ^{86}Sr is 6.8%. The extracted PNCS distribution was consistent with the TALYS calculations, validating the proposed extraction method.

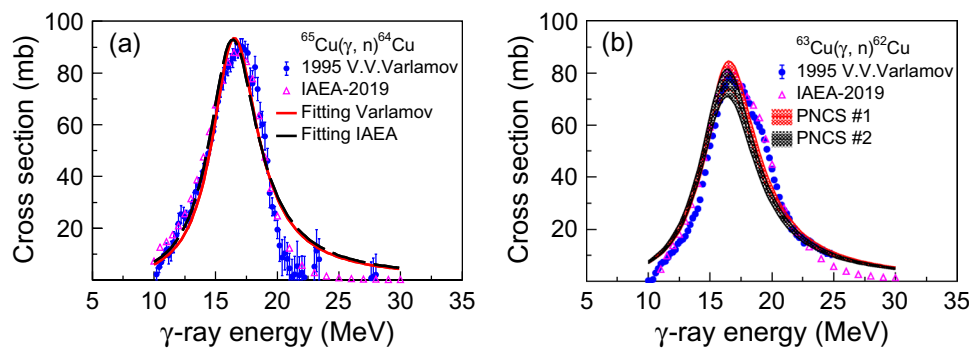


Fig. 3 (Color online) **a** Experimental and evaluated PNCS data for ^{65}Cu [25, 33] and the resultant fitted Lorentzian-like distributions and **b** predicted PNCS distributions for ^{63}Cu and the experimental and evaluated PNCS data for comparison. PNCS #1 and PNCS #2 repre-

sent the PNCS distributions extracted from the Lorentzian parameters fitted from experimental and evaluated data, respectively. The shadow area indicates the uncertainty of the extracted PNCS distributions for ^{63}Cu

Table 2 Lorentzian parameters fitted using experimental and evaluated PNCS data

Reaction	Cross section data	Fitted Lorentzian parameters		
		E_m (MeV)	Γ (MeV)	σ_m (mb)
$^{65}Cu(\gamma, n)^{64}Cu$	1995 V. V. Varlamov	16.53 ± 0.04	4.52 ± 0.08	96.63 ± 1.09
$^{65}Cu(\gamma, n)^{64}Cu$	2019 IAEA evaluation	16.39 ± 0.10	4.81 ± 0.27	93.03 ± 3.53
$^{63}Cu(\gamma, n)^{62}Cu$	2019 IAEA evaluation	16.86 ± 0.08	5.51 ± 0.22	84.77 ± 2.17

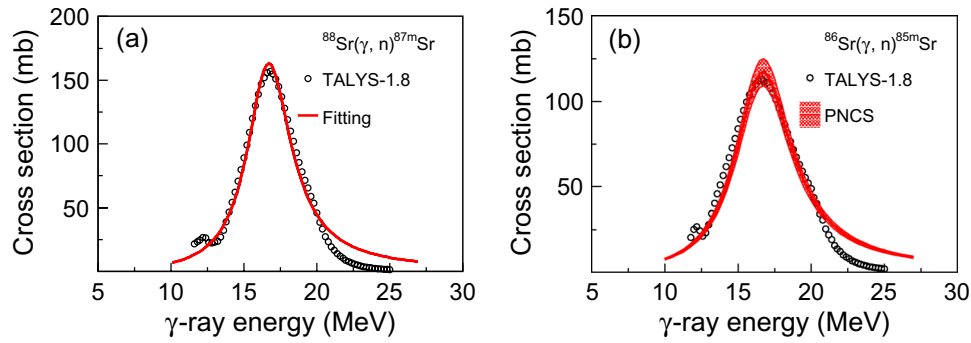


Fig. 4 (Color online) **a** TALYS-calculated PNCS data for ^{88}Sr [34] and the resultant fitted Lorentzian-like distributions, and **b** predicted PNCS distributions for ^{86}Sr and the TALYS-calculated PNCS data for

comparison. PNCS represents the PNCS distribution extracted from the Lorentzian parameters fitted from TALYS data. The shadow area indicates the uncertainty of the predicted PNCS distribution for ^{86}Sr

Table 3 Lorentzian parameters fitted using TALYS-calculated PNCS data

Reaction	Cross section data	Fitted Lorentzian parameters		
		E_m (MeV)	Γ (MeV)	σ_m (mb)
$^{88}\text{Sr}(\gamma, n)^{87m}\text{Sr}$	TALYS calculation	16.72 ± 0.04	3.71 ± 0.10	163.13 ± 3.08
$^{86}\text{Sr}(\gamma, n)^{85m}\text{Sr}$	TALYS calculation	16.51 ± 0.05	4.74 ± 0.14	117.74 ± 2.36

Fig. 5 (Color online) 30 isotopes with corresponding PNCS distributions that are suitable for extraction using our proposed method. The transversal and longitudinal coordinates indicate the name of these isotopes and their natural abundances, respectively. The color bar presents the half-lives of the residual nuclei

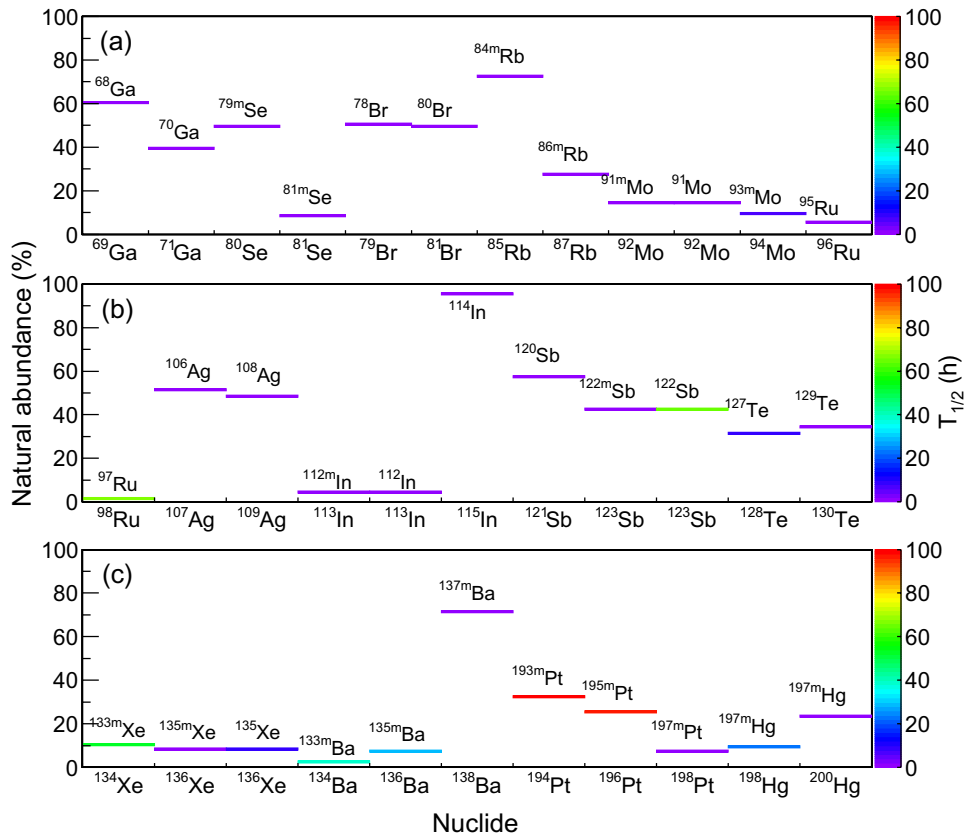


Table 4 Detailed information for 30 isotopes with corresponding PNCS distributions that are suitable for extraction using our proposed method. A large uncertainty means the experimental data have an uncertainty larger than 10%

Target nuclide	Abundance (%)	Residual nuclide	$T_{1/2}$ (h)	E_γ (keV)	I_γ (%)	Experimental data
^{69}Ga	60.11	^{68}Ga	1.13	1077.3	3.2	Not available
^{71}Ga	39.89	^{70}Ga	0.35	1039.5	0.7	Not available
^{80}Se	49.6	$^{79\text{m}}\text{Se}$	0.07	95.7	9.5	Large uncertainty
^{82}Se	8.73	$^{81\text{m}}\text{Se}$	0.95	103.1	12.8	Large uncertainty
^{79}Br	50.69	^{78}Br	0.11	613.7	13.6	Large uncertainty
^{81}Br	49.31	^{80}Br	0.29	616.3	6.7	Large uncertainty
^{85}Rb	72.17	$^{84\text{m}}\text{Rb}$	0.34	248.0	63.0	Acceptable uncertainty
^{87}Rb	27.83	$^{86\text{m}}\text{Rb}$	0.02	556.1	98.2	Not available
^{92}Mo	14.53	$^{91\text{m}}\text{Mo}$	0.02	652.9	48.2	Large uncertainty
^{92}Mo	14.53	^{91}Mo	0.26	511.0	187.5	Large uncertainty
^{94}Mo	9.15	$^{93\text{m}}\text{Mo}$	6.85	684.7	99.9	Not available
^{96}Ru	5.54	^{95}Ru	1.64	336.4	69.9	Large uncertainty
^{98}Ru	1.87	^{97}Ru	67.92	215.7	85.6	Not available
^{107}Ag	51.84	^{106}Ag	0.4	511.0	118.0	Acceptable uncertainty
^{109}Ag	48.16	^{108}Ag	0.04	632.9	1.8	Large uncertainty
^{113}In	4.29	$^{112\text{m}}\text{In}$	0.34	156.6	13.3	Not available
^{113}In	4.29	^{112}In	0.25	617.5	6.7	Not available
^{115}In	95.71	^{114}In	0.02	1299.8	0.2	Large uncertainty
^{121}Sb	95.71	^{120}Sb	0.26	511.0	82.0	Large uncertainty
^{123}Sb	42.79	$^{122\text{m}}\text{Sb}$	0.07	61.4	55.0	Not available
^{123}Sb	42.79	^{122}Sb	65.52	564.2	70.7	Not available
^{128}Te	31.74	^{127}Te	9.35	417.9	1.0	Large uncertainty
^{130}Te	34.08	^{129}Te	1.16	459.6	7.7	Large uncertainty
^{134}Xe	10.44	$^{133\text{m}}\text{Xe}$	52.8	233.2	10.1	Not available
^{136}Xe	8.86	$^{135\text{m}}\text{Xe}$	0.25	526.6	80.4	Large uncertainty
^{136}Xe	8.86	^{135}Xe	9.14	249.8	90.0	Acceptable uncertainty
^{134}Ba	2.42	$^{133\text{m}}\text{Ba}$	38.93	275.9	17.7	Large uncertainty
^{136}Ba	7.85	$^{135\text{m}}\text{Ba}$	28.7	268.2	16.0	Large uncertainty
^{138}Ba	71.70	$^{137\text{m}}\text{Ba}$	0.04	661.7	89.9	Large uncertainty
^{194}Pt	32.86	$^{193\text{m}}\text{Pt}$	103.92	66.8	7.21	Not available
^{196}Pt	25.21	$^{195\text{m}}\text{Pt}$	96.24	98.9	11.7	Not available
^{198}Pt	7.36	$^{197\text{m}}\text{Pt}$	23.8	346.5	11.1	Large uncertainty
^{198}Hg	9.97	$^{197\text{m}}\text{Hg}$	1.59	134.0	33.5	Large uncertainty
^{200}Hg	23.10	$^{199\text{m}}\text{Hg}$	0.71	158.3	52.3	Not available

4 Discussions

The proposed extraction method has the following advantages: First, an accurate knowledge of the bremsstrahlung spectrum induced by intense lasers is not required because the reaction yield ratio method is used. When employing intense laser-accelerated electrons to produce bremsstrahlung radiation, they can still be subtracted using our extraction method although shot-to-shot variations exist in the bremsstrahlung spectrum and intensity. Second, it is not necessary to scan the incident photon energy, which generally happens in both the apparatus method using a

quasi-monoenergetic photon beam and the mathematical method using classical bremsstrahlung measurements. Third, PNCS distributions can be successfully extracted within a very short time, within seconds, when using a state-of-the-art laser plasma-based bremsstrahlung source [29, 30]. Finally, it should be noted that any gamma source with a continuous spectrum covering the central GDR region is suitable for gamma activation. In general, gamma rays can be produced using either bremsstrahlung or LCS. When the spectral distribution of the gamma source is $n_\gamma(E) = n_\gamma(0)f(E)$, where $f(E)$ is an energy-dependent function, Eq. (4) can then be written as $\frac{Y_{A'}}{Y_{B'}} = \frac{n_A}{n_B} \cdot \frac{\int \sigma_A(E)f(E)dE}{\int \sigma_B(E)f(E)dE}$.

The approximations given in Eq. (4) remain valid because of the similar values of E_m and Γ for the same nuclides as adjacent A , as discussed above.

However, the PNCS distributions of the studied isotopes must have Lorentzian-like shapes. This was a prerequisite for validating the proposed extraction method. Here, it is interesting to discuss how precisely the PNCS distribution can be described by a Lorentzian shape. Generally, a Lorentzian-like shape accurately describes the PNCS distribution in the central GDR energy range but fails in the high-energy tail [16]. In our study, the relative difference between the predicted PNCS (integrated over the 10–25 MeV energy range) and the benchmarked PNCS was determined to be 3.2% for ^{63}Cu and 3.9% for ^{86}Sr . However, it increases to more than 50% in the high-energy range of 20–25 MeV. Meanwhile, successful extraction of the PNCS distribution relies on the fact that the residual nuclide should have a suitable half-life (note that a relatively long half-life is also acceptable), which is helpful for detecting characteristic emissions after target activation. To obtain a high reaction yield and reduce statistical uncertainty, the offline-detected characteristic emissions should have relatively large branching intensities and detection efficiencies. In addition, isotopes undergoing photonuclear reactions should have acceptable natural abundances because natural metal targets are commonly used for irradiation. Based on these considerations, the PNCS distributions of 30 isotopes were predicted using the proposed extraction method. Figure 5 shows the natural abundances of these isotopes and half-lives of the residual nuclei. Approximately half of them had PNCS distributions, leading to isomeric states of the residual nuclei. More detailed information regarding the target and residual nuclides is presented in Table 4. Their experimental PNCS data for 18 isotopes exhibited large uncertainty (>10%). The PNCS data for ^{85}Rb , ^{107}Ag , ^{136}Xe , and ^{153}Eu have acceptable uncertainties because these isotopes are categorized as either medical or other types of materials [1], which requires an uncertainty of less than 10%.

5 Conclusion

We proposed an effective method for obtaining the peak cross section and extracting the PNCS distribution using the gamma activation and reaction yield ratio method. The PNCS distributions of ^{63}Cu and ^{86}Sr isotopes (leading to $^{85\text{m}}\text{Sr}$ isotope production) were successfully extracted using the proposed extraction method. The uncertainty of this method was maintained within 7%. The extracted PNCS distributions and the available PNCS data (or TALYS calculations) were compared to validate the proposed extraction method. The prerequisites and merits of the extraction method and the possibility of predicting PNCS distributions

for 30 isotopes were also discussed. The proposed extraction method could be complementary to the available sophisticated methods, including the mathematical method using bremsstrahlung measurements and the apparatus method with positron annihilation in flight and LCS photon spectrum. In the near future, we plan to perform gamma activation experiments using laser plasma-driven bremsstrahlung sources and extract the PNCS distributions for a list of isotopes with relatively large abundances and significant characteristic emissions after short-term irradiation.

Acknowledgements We express our gratitude to the XingGuang III operation team for their support.

Author contributions All authors contributed to the study conception and design. Material preparation, data collection and analysis were performed by Zhi-Cai Li, Yue Yang, Zong-Wei Cao, Xin-Xiang Li, Yun Yuan, Zong-Qing Zhao, Gong-Tao Fan, Hong-Wei Wang and Wen Luo. The first draft of the manuscript was written by Zhi-Cai Li, and all authors commented on previous versions of the manuscript. All authors read and approved the final manuscript.

Data availability The data that support the findings of this study are openly available in Science Data Bank at <https://doi.org/10.57760/sciencedb.j00186.00302> and <https://cstr.cn/31253.11.sciencedb.j00186.00302>.

Declarations

Conflict of interest Hong-Wei Wang is an editorial board member for Nuclear Science and Techniques and was not involved in the editorial review, or the decision to publish this article. All authors declare that there are no competing interests.

References

1. T. Kawano, Y.S. Cho, P. Dimitriou et al., IAEA photonuclear data library 2019. Nucl. Data Sheets **163**, 109–162 (2020). <https://doi.org/10.1016/j.nds.2019.12.002>
2. H.Y. Lan, T. Song, Z.H. Luo et al., Isotope-sensitive imaging of special nuclear materials using computer tomography based on scattering nuclear resonance fluorescence. Phys. Rev. Appl. **16**, 054048 (2021). <https://doi.org/10.1103/PhysRevApplied.16.054048>
3. X.Y. Sun, W. Luo, H.Y. Lan et al., Transmutation of long-lived fission products in an advanced nuclear energy system. Sci. Rep. **12**, 2240 (2022). <https://doi.org/10.1038/s41598-022-06344-y>
4. X.L. Wang, Z.Y. Xu, W. Luo et al., Transmutation prospect of long-lived nuclear waste induced by high-charge electron beam from laser plasma accelerator. Phys. Plasmas **24**, 093105 (2017). <https://doi.org/10.1063/1.4998470>
5. Z.G. Ma, H.Y. Lan, W.Y. Liu et al., Photonuclear production of medical isotopes $^{62,64}\text{Cu}$ using intense laser-plasma electron source. Matter Radiat. Extremes **4**, 064401 (2019). <https://doi.org/10.1063/1.5100925>
6. W. Luo, Production of medical radioisotope ^{64}Cu by photoneutron reaction using ELI-NP γ -ray beam. Nucl. Sci. Tech. **27**, 96 (2016). <https://doi.org/10.1007/s41365-016-0094-6>
7. H.Y. Lan, W. Luo, Y. Xu et al., Feasibility of studying astrophysically important charged-particle emission with the variable energy γ -ray system at the Extreme Light Infrastructure-Nuclear Physics

- facility. *Phys. Rev. C* **105**, 044618 (2022). <https://doi.org/10.1103/PhysRevC.105.044618>
8. H.Y. Lan, Y. Xu, W. Luo et al., Determination of the photodisintegration reaction rates involving charged particles: Systematic calculations and proposed measurements based on the facility for Extreme Light Infrastructure-Nuclear Physics. *Phys. Rev. C* **98**, 054601 (2018). <https://doi.org/10.1103/PhysRevC.98.054601>
 9. W. Luo, D.L. Balabanski, D. Filipescu, A data-based photonuclear simulation algorithm for determining specific activity of medical radioisotopes. *Nucl. Sci. Tech.* **27**, 113 (2016). <https://doi.org/10.1007/s41365-016-0111-9>
 10. D. Habs, U. Koster, Production of medical radioisotopes with high specific activity in photonuclear reactions with γ -beams of high intensity and large brilliance. *Appl. Phys. B* **103**, 501 (2011). <https://doi.org/10.1007/s00390-010-4278-1>
 11. W. Luo, M. Bobeica, I. Gheorghe et al., Estimates for production of radioisotopes of medical interest at extreme light infrastructure-nuclear physics facility. *Appl. Phys. B* **122**, 8 (2016). <https://doi.org/10.1007/s00340-015-6292-9>
 12. A.L. Nichols, R. Capote, Nuclear data for medical applications—recent developments and future requirements. *Nucl. Data Sheets* **120**, 239 (2014). <https://doi.org/10.1016/j.nds.2014.07.056>
 13. K.M. El-Azony, N.M.A. Mohamed, D.A. Aloraini, Advantages and disadvantages of nuclear reactions used in reactors or cyclotrons, in addition to a theoretical study based on photodisintegration on natural indium for ^{111}Ag production. *Nucl. Sci. Tech.* **33**, 14 (2022). <https://doi.org/10.1007/s41365-022-00991-6>
 14. A. Zilges, D.L. Balabanski, J. Isaak et al., Photonuclear reactions—From basic research to applications. *Prog. Part. Nucl. Phys.* **122**, 103903 (2022). <https://doi.org/10.1016/j.ppnp.2021.103903>
 15. H.W. Wang, G.T. Fan, L.X. Liu et al., Commissioning of laser electron gamma beamline SLEGS at SSRF. *Nucl. Sci. Tech.* **33**, 87 (2022). <https://doi.org/10.1007/s41365-022-01076-0>
 16. K.J. Chen, L.X. Liu, Z.R. Hao et al., Simulation and test of the SLEGS TOF spectrometer at SSRF. *Nucl. Sci. Tech.* **34**, 47 (2023). <https://doi.org/10.1007/s41365-023-01194-3>
 17. H. Utsunomiya, I. Gheorghe, D.M. Filipescu et al., Direct neutron-multiplicity sorting with a flat-efficiency detector. *Nucl. Inst. Meth. A.* **871**, 135 (2017). <https://doi.org/10.1016/j.nima.2017.08.001>
 18. H.Y. Lan, D. Wu, J.X. Liu et al., Photonuclear production of nuclear isomers using bremsstrahlung induced by laser wakefield electrons. *Nucl. Sci. Tech.* **34**, 74 (2023). <https://doi.org/10.1007/s41365-023-01219-x>
 19. B.L. Berman, S.C. Fultz, Measurements of the giant dipole resonance with monoenergetic photons. *Rev. Mod. Phys.* **47**, 713 (1975). <https://doi.org/10.1103/RevModPhys.47.713>
 20. H. Utsunomiya, S. Hashimoto, S. Miyamoto, The γ -ray beam-line at NewSUBARU. *Nucl. Phys. News* **25**, 25 (2015). <https://doi.org/10.1080/10619127.2015.1067539>
 21. N. Otuka, E. Dupont, V. Semkova et al., Towards a more complete and accurate experimental nuclear reaction data library (EXFOR): international collaboration between nuclear reaction data centres (NRDC). *Nucl. Data Sheets* **120**, 272 (2014). <https://doi.org/10.1016/j.nds.2014.07.065>
 22. S. Goriely, P. Dimitriou, M. Wiedeking et al., Reference database for photon strength functions. *Eur. Phys. J. A* **55**, 172 (2019). <https://doi.org/10.1140/epja/i2019-12840-1>
 23. J. Magill, H. Schwoerer, H. Ewald et al., Laser transmutation of iodine-129. *Appl. Phys. B* **77**, 387–390 (2003). <https://doi.org/10.1007/s00390-003-1306-4>
 24. R. Bergère, H. Beil, P. Carlos et al., Sections efficaces photon-neutroniques de I, Ce, Sm. Er et Lu. *Nucl. Phys. A* **133**, 417–437 (1969). [https://doi.org/10.1016/0375-9474\(69\)90644-7](https://doi.org/10.1016/0375-9474(69)90644-7)
 25. V.V. Varlamov, N.G. Efimkin, B.S. Ishkhanov et al., Evaluation of $^{63,65}\text{Cu}(\gamma, np)$ and $^{63,65}\text{Cu}(\gamma, p)$ reaction cross sections in the energy range of giant dipole resonance and isospin splitting of the GDR of Cu nuclei. *Bull. Rus. Acad. Sci. Phys.* **59**, 911 (1995)
 26. A.M. Goryachev, G.N. Zalesnyy, The studying of the photoneutron reactions cross sections in the region of the giant dipole resonance in zinc, germanium, selenium, and strontium isotopes. *Voprosy Teoreticheskoy i Yadernoy Fiziki.* **8**, 121 (1982). <http://www-nds.iaea.org/EXFOR/M0070.021>
 27. C. Plaisir, F. Hannachi, F. Gobet et al., Measurement of the $^{85}\text{Rb}(\gamma, n)^{84m}\text{Rb}$ cross-section in the energy range 10–19 MeV with bremsstrahlung photons. *Eur. Phys. J. A* **48**, 68 (2012). <https://doi.org/10.1140/epja/i2012-12068-7>
 28. TENDL-2021 nuclear data library. https://tendl.web.psi.ch/tendl_2021/gamma_html/gamma.html. Accessed 18 Mar 2023
 29. O.N. Rosmej, M. Gyrdymov, M.M. Günther et al., High-current laser-driven beams of relativistic electrons for high energy density research. *Plasma Phys. Control. Fusion.* **62**, 115024 (2020). <https://doi.org/10.1088/1361-6587/abb24e>
 30. J.P. Couperus, R. Pausch, A. Köhler et al., Demonstration of a beam loaded nanocoulomb-class laser wake field accelerator. *Nat. Commun.* **8**, 487 (2017). <https://doi.org/10.1038/s41467-017-00592-7>
 31. H. Cheng, B.H. Sun, L.H. Zhu et al., Measurements of $^{160}\text{Dy}(p, \gamma)$ at Energies Relevant for the Astrophysical γ Process. *Astrophysical J.* **915**, 78 (2021). <https://doi.org/10.3847/1538-4357/ac00b1>
 32. Z.W. Cao, W. Qi, H.Y. Lan et al., Experimental study of medical isotopes $^{62,64}\text{Cu}$ and ^{68}Ga production using intense picosecond laser pulse. *Plasma Phys. Control. Fusion.* **65**, 055007 (2023). <https://doi.org/10.1088/1361-6587/acc090>
 33. JANIS Web. www.oecd-nea.org/janisweb/book/gammas. Accessed 19 Mar 2023
 34. A.J. Koning, S. Hilaire, M.C. Duijvestijn, TALYS: comprehensive nuclear reaction modeling, in *AIP Conference Proceedings* vol. 769, pp. 1154–1159 (2005). <https://doi.org/10.1063/1.1945212>

Springer Nature or its licensor (e.g. a society or other partner) holds exclusive rights to this article under a publishing agreement with the author(s) or other rightsholder(s); author self-archiving of the accepted manuscript version of this article is solely governed by the terms of such publishing agreement and applicable law.